Available online at www.sciencedirect.com
SCIENCE DIRECT®
Journal of Power Sources 140 (2005) 139–144
JOURNAL OF POWER SOURCES
www.elsevier.com/locate/jpowsour

Short communication

Effect of electrode structure on performance of Si anode in Li-ion batteries: Si particle size and conductive additive

Wei-Ren Liu[a], Zheng-Zao Guo[b], Wen-Shiue Young[a], Deng-Tswen Shieh[b], Hung-Chun Wu[b], Mo-Hua Yang[b], Nae-Lih Wu[a,*]

[a] *Department of Chemical Engineering, National Taiwan University, Taipei, Taiwan 106, ROC*
[b] *Materials Research Laboratories, ITRI, Chutung, Hsin-Chu, Taiwan 310, ROC*

Received 12 May 2004; accepted 21 July 2004
Available online 27 October 2004

Abstract

The effects of Si particle size and the amount of carbon-based conductive additive (CA) on the performance of a Si anode in a Li-ion battery are investigated by adopting combinations of two different Si particle sizes (20 and 3 μm on average) and CA contents (15 and 30 wt.%), respectively. The CA contains graphitic flakes and nano-sized carbon black. Cyclic voltammetry, charge–discharge tests, scanning electron microscopy and X-ray diffraction establish that the CA content has a profound effect on the cycle-life and irreversible capacity of the Si anode. The former increases, while the latter decreases significantly with increasing CA content. Reducing the particle size of Si, on the other hand, facilitates the alloying/de-alloying kinetics. For instance a cycle-life of over 50 cycles with >96% capacity retention at a charge capacity of 600 mAh per g-Si has been demonstrated by adopting of 30 wt.% CA and 3 μm Si particles.

Keywords: Lithium ion battery; Silicon; Anode; Cycle-life

1. Introduction

As an anode for the Li-ion battery, Si possesses a maximum Li uptake of Li/Si = 4.4/1.0, which corresponds to a theoretical capacity of 4200 mAh g^{-1}. This is a significant improvement over the 372 mAh g^{-1} provided by graphite. These are, however, shortcomings when using silicon, namely, a dramatic volumetric variation during charge–discharge (i.e., alloy–de-alloy) cycling and the intrinsic poor conductivity of Si. The former is claimed to cause poor cycle-life, and the latter results in high resistance and low Li uptake. Many attempts have been made recently to solve these problems by coating the surfaces of the Si particles with different conducting materials via different techniques [1–12]. For instance, Yoshio et al. [1–3] demonstrated that graphitic coating of Si by thermal vapour deposition enabled tens cycles to be sustained at charging depths up to 1000 mAh per g-Si. This performance was far superior to un-coated silicon that gave a cycle-life of typically less than a few cycles. Less improvement was achieved by introducing other secondary and/or coating materials, such as metals, oxides and nitrides [9–12]. Ironically, there have been few reports of systematic investigations of the effects due to the 'original' constituents, such as the Si particles and conductive additives, that are conventionally employed in constructing a Si anode. As these constitutents are expected to continue to be the major elements of the structure of the Si anode, even when a new secondary/coating material is introduced, optimizing their properties is crucial to the resulting performance.

This work examines the effects of the particle size of Si and the amount of conductive additive (CA) on the performance, particularly cycle-life and irreversible capacity, of the Si anode. In brief, it is found that the CA content has a much more profound effect than the Si particle-size on cycle-life, which increases with increasing CA content. Electrodes with

* Corresponding author. Tel.: +886 2 2362 7158.
E-mail address: nlw001@ntu.edu.tw (N.-L. Wu).

0378-7753/$ – see front matter © 2004 Elsevier B.V. All rights reserved.
doi:10.1016/j.jpowsour.2004.07.032

high (30 wt.%) CA content yield very low (<60 mAh g^{-1}) irreversible capacities even during the initial cycles. Reducing the Si particle size, on the other hand, effectively facilitates the charge–discharge kinetics.

2. Experimental

The particle-size effect was investigated by using Si powders with two different size-distributions. The as-received Si powder (99.9%, Aldrich), which will be referred to as the 20 μm-powder, has a size-distribution that peaks at ∼20 μm (curve 1, Fig. 1) and contains ∼77% of the particles with a size between 10 and 40 μm, as determined by light-scattering analysis (LS-230; Coulter). The other batch, the 3 μm powder (curve 2, Fig. 1), was obtained by ball-milling the 20 μm powder in a polyethylene jar that contained two different sizes of Al_2O_3 balls, i.e., one with a 5 mm and the other with a 2 mm diameter. The rotation speed was 300 rpm and the milling was conducted for 24 h. The milled powder has a bimodal particle-size distribution with an average size of ∼3 μm and less than 15% of the particles are larger than 5 μm.

Si electrodes containing different proportions of the Si particles and CA were prepared on Cu-foil current-collectors with dried film thicknesses of ∼40 μm. The CA was a mixture of graphitic flakes (KS6, 3 μm) and nano-sized carbon black (Super P, 40 nm) at a weight ratio of 5:1. CR2032 coin cells were fabricated; each comprised a Si electrode with a Li foil counter-electrode and an electrolyte of 1 M $LiPF_6$ in ethylene carbonate (EC): ethyl methyl carbonate (EMC) (1:2). All potentials are reported with respect to Li/Li^+. Cyclic voltammetry (CV) analysis was performed between 0.05 and 3.0 V at 10 mV min^{-1}. A typical charge–discharge (C–D) cycle consisted of these steps, viz: (i) charging at a constant-current (CC) of 0.3 mA mg^{-1} until either the selected specific capacity (mAh g^{-1}) or zero potential was reached; (ii) discharging at 0.3 mA mg^{-1} until the cut-off voltage (1.2 V) was reached; (iii) an equilibrating period of 5 h was imposed at the end of the first charging.

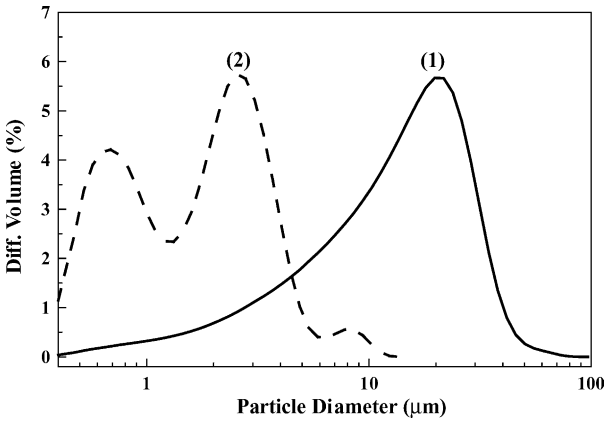

Fig. 1. Particle-size distributions of two silicon powders: (1) the 20 μm powder and (2) the 3 μm powder.

For each specimen, the particle morphology and electrode cross-section were examined by scanning electron microscopy (SEM; HITACHI S-800). X-ray diffraction (XRD) was carried out on a Mac-Science/MXP diffractometer with Cu Kα radiation.

3. Results and discussion

The CV curves for electrodes that differ in either Si particle size or CA content are presented in Fig. 2(a) through (C). The electrodes will hereafter be designated by their average Si particle size (3 or 20 μm) and the weight percentage of the CA. For the 20 μm–30% electrode (Fig. 2(a)), the first CV cycle does not showed any distinct reduction (Li alloying) peak but a broad dimple between 0.3 and 0.8 V, followed by strong reduction towards zero potential. The broad dimple is in fact observed for most electrodes and, in all cases, it is irreversible and occurs only during the first cycle. Its occurrence is likely due to the reaction between Li ions and surface-adsorbed oxygen-containing species, such as –O or –OH. The lack of any distinct reduction peak indicates sluggish alloying kinetics. For the oxidation branch of the curve, one shoulder and two distinct peaks, designated respectively as OX(0.20 V), OX(0.35 V) and OX(0.60 V), are observed at ∼0.20, 0.35 and 0.60 V, respectively. The appearance of these peaks may suggest that de-alloying proceeds faster than alloying. Upon further cycling, a broad reduction shoulder at ∼0.15 V (designated as RE(0.15 V)) starts to evolve, which suggests a slight increase in the alloying kinetics with increasing cycling. SEM examination of the electrode surface reveals breaking-up of the Si particles into agglomerates of 50–60 nm nano-particles (Fig. 3). Thus, the increase in the reaction kinetics upon cycling may be associated with the formation of smaller particles, as discussed below.

Reducing the particle size of Si in the starting electrode results in several significant differences in CV characteristics, as shown by the 3 μm–30% electrode (Fig. 2(b)). First, a decrease in particle size would result in an increase in the particle|electrolyte interfacial area. This leads to an overall increase in the responding current under a fixed sweep rate. Second, a much stronger RE(0.15 V) peak is established, and there is also a large increase in the OX(0.60 V) intensity. These features indicate accelerated alloying and de-alloying kinetics, respectively, that can be attributed to a shorter solid-state diffusion length for Li ions.

Finally, reducing the CA content (e.g., the 3 μm–15% electrode in Fig. 2(c)) is found to cause a shift towards lower and higher potentials for the reduction and oxidation peaks, respectively. This may be due to polarization that arises from increased electrode resistance. Notably, the profile of the oxidation trace is altered as the oxidation peaks are shifted to different extents.

For cycle-life tests, Fig. 4(a)–(e) summarize the capacity data as a function of cycle number, and Fig. 5(a) and (b) show the charge–discharge (C-D) curves for selected cycles. The

following points are noted. First, in all cases, it typically takes a couple of C-D cycles for the electrodes to reach the designated charging level. As also indicated by the CV data, this is due to a gradual acceleration of the charging kinetics with cycling. Second, the electrodes exhibit two distinct types of cycling stability. Irrespective of particle size, the cells with 15 wt.% CA display an exponential decay in both charge and discharge capacities in less than five cycles after the designated charge level (600 mAh g^{-1}) is reached. On the other hand, those with 30 wt.% CA give better than 90% capacity retention after 50 cycles. For the same CA content, the performance of the cells made of the 3 μm powder is slightly superior to that of cells with 20 μm-powder. With the combination of 3 μm Si and 30% CA, >96% capacity is retained after 50 cycles at a charge capacity of 600 mAh per g-Si (Fig. 4(d)), or 90% capacity up to ∼45 cycles at 800 mAh per g-Si (Fig. 4(e)). A third noticeable feature is that the irreversible capacities for the 30%-CA electrodes during first couple of cycles are small, i.e., less than 60 mAh per g-Si. Large irresversible capacities, in the range of 200–300 mAh per g-Si, occurr only for the 15%-CA electrodes, which also

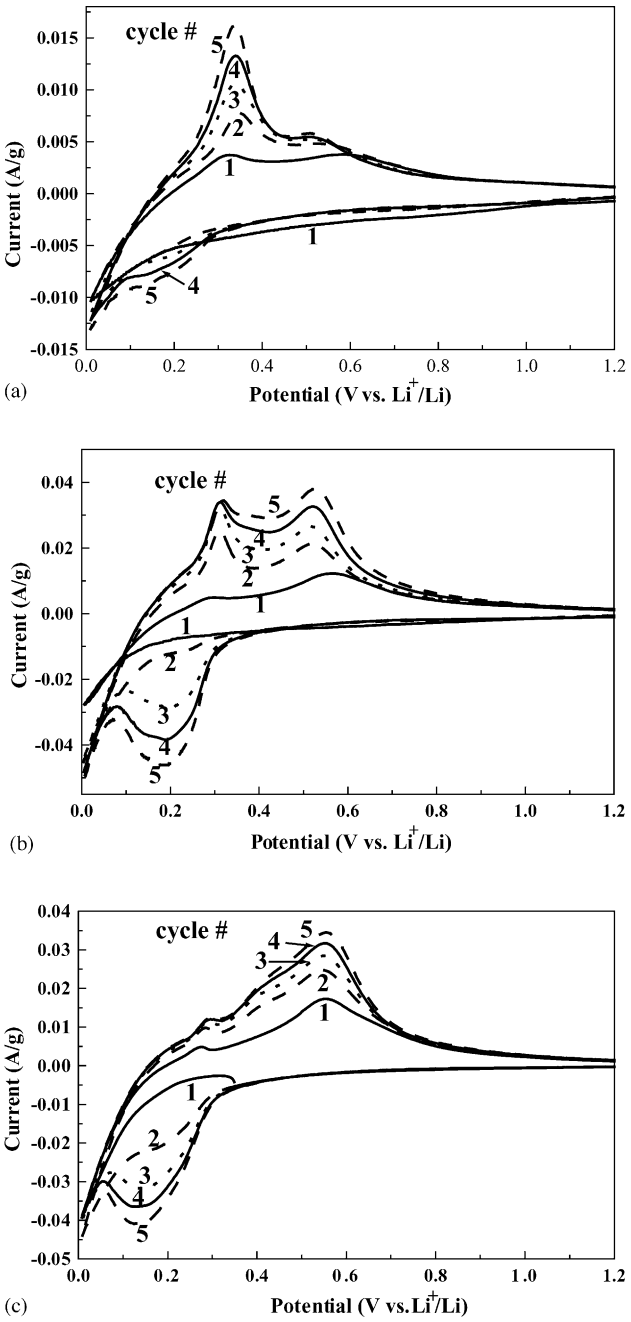

Fig. 2. CV curves for different Si electrodes: (a) 20 μm–15%; (b) 3 μm–30%; (c) 3 μm–15%.

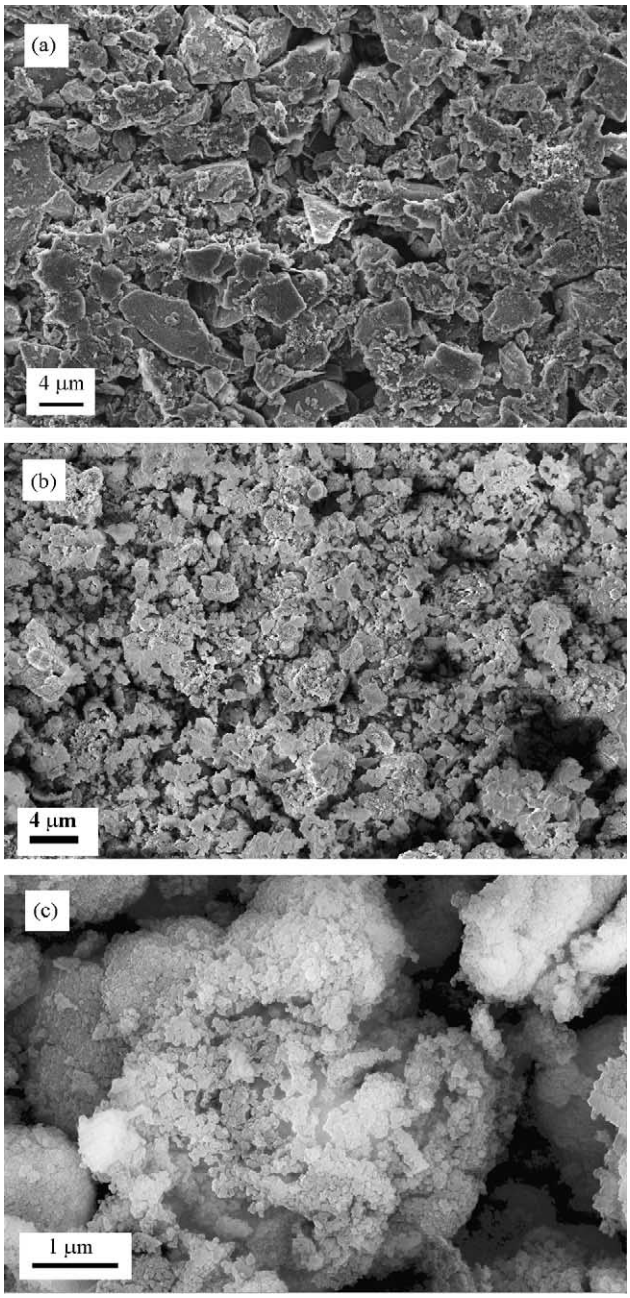

Fig. 3. SEM micrographs of the Si anode surfaces (a) before and (b) (c) after charge–discharge tests.

showed poor cycle-life. Clearly, these large capacity losses are not due to formation of a solid electrolyte interface (SEI) film. Rather, they arise because part of the Li alloyed with Si cannot be released due to poor contact with CA upon charge–discharge, as discussed below.

The C-D curves show that the 15%-electrode exhibits a charging plateau at significantly lower potentials than the 30%-electrode (Fig. 5(a)). This suggests a greater polarization associated with a lower CA content. This, as described earlier, was also evident in CV curves (Fig. 2(c)). Furthermore, the charging plateau shifts progressively to lower potentials and the charging capacity decrease accordingly with cycling. The ever increasing polarization is believed to arise from a gradual disintegration of the electrode structure, which causes a concomitant increase in the impedance of the electrode. SEM analysis of the cross-section of the electrodes reveals a significant expansion in electrode thickness after C-D cycling (Fig. 6). That is, after the electrode expands

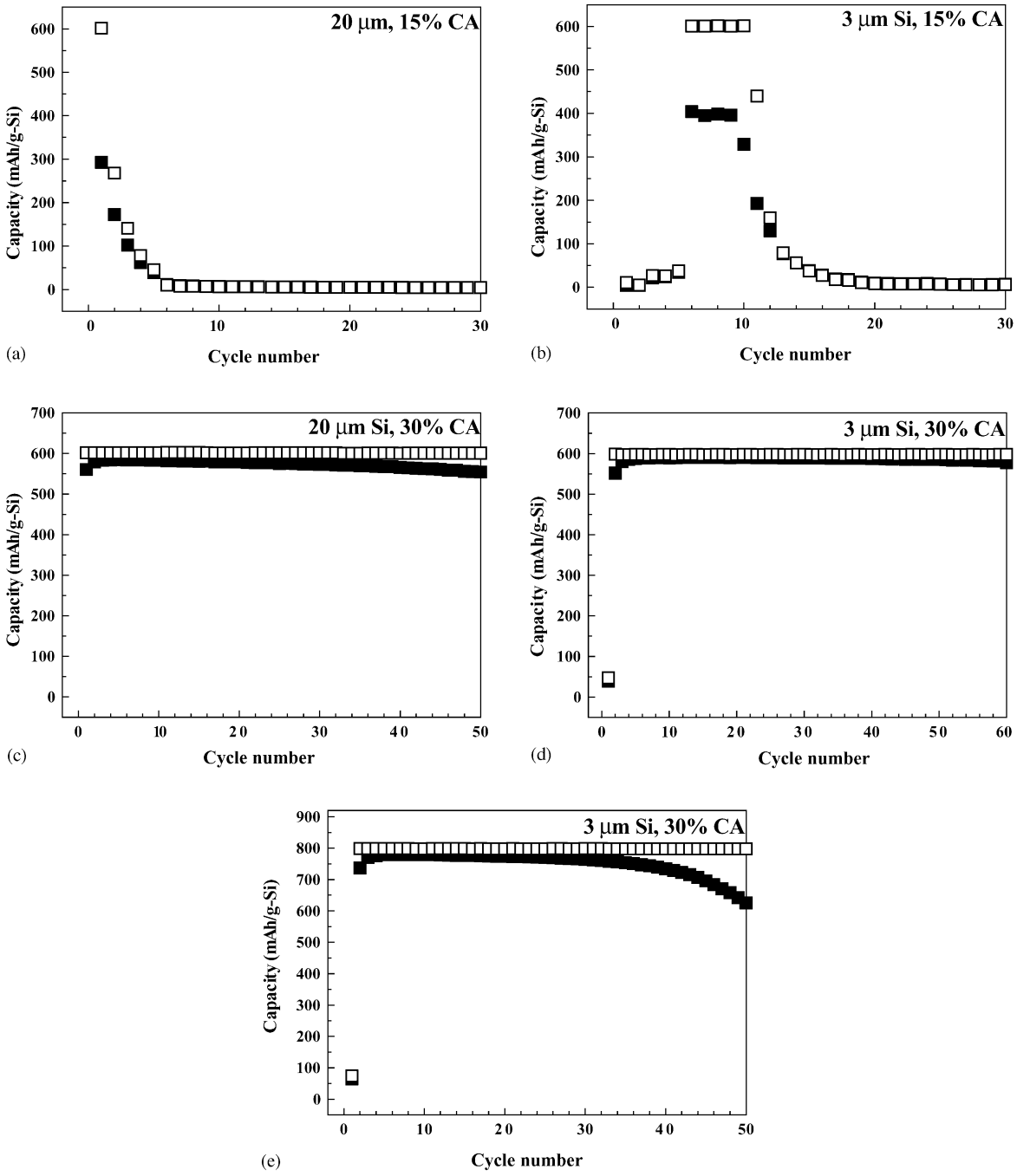

Fig. 4. Cycling performance of coin cells consisting of different Si electrodes: (a) 20 μm–15%; (b) 3 μm–15%; (c) 20 μm–30%; (d) 3 μm–30% at charge depth of 600 mAh per g-Si; (e) 3 μm–30% at 800 mAh per g-Si. (key: (□) charge capacity; (■) discharge capacity).

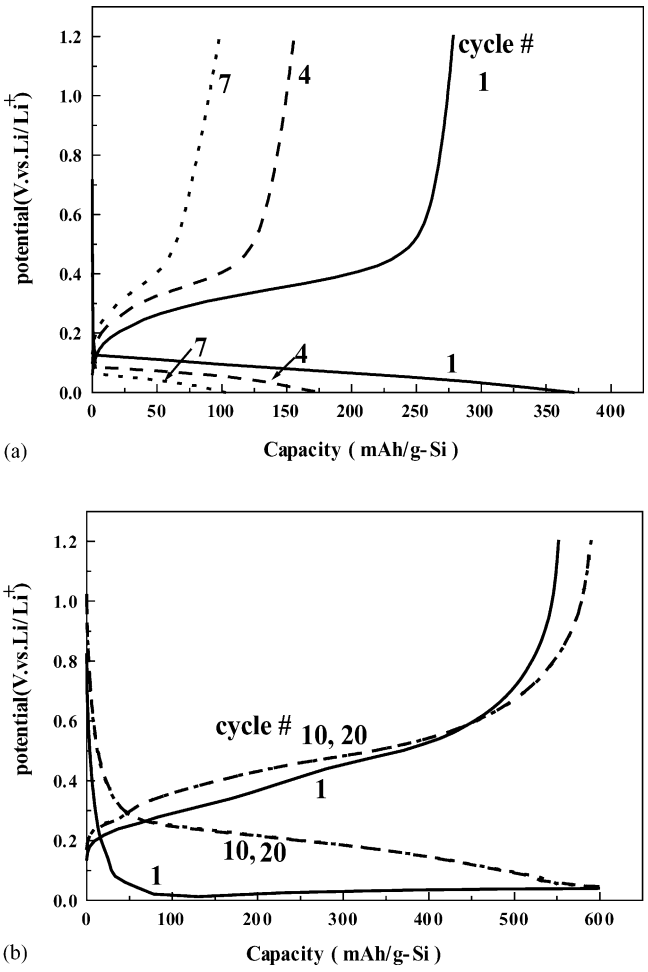

Fig. 5. The charge–discharge curves of selected cycles for (a) 20 μm–15% and (b) 3 μm–30% electrodes.

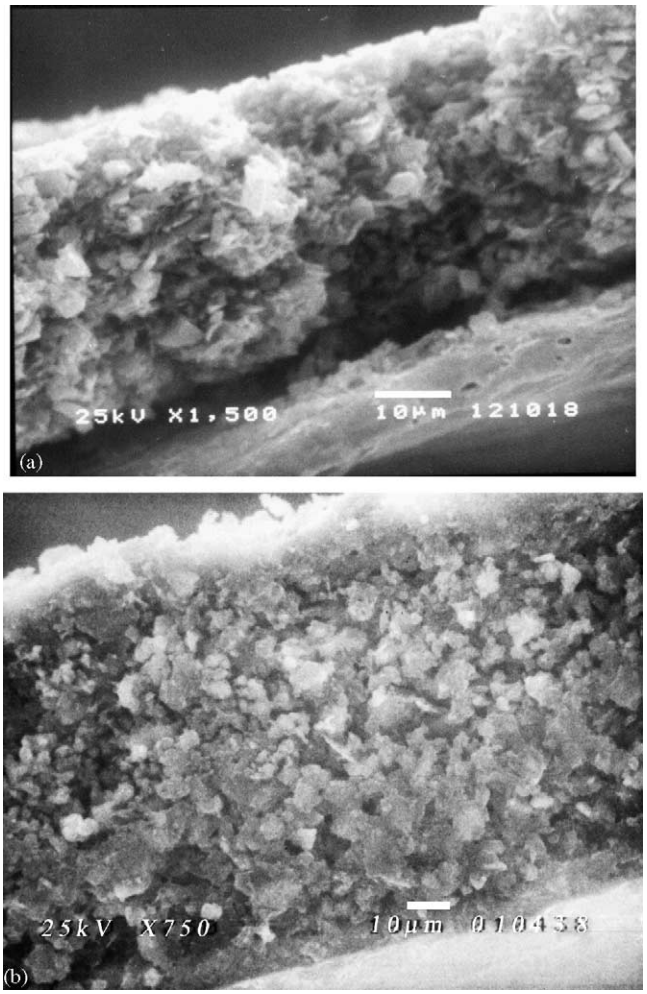

Fig. 6. SEM of cross-sections of Si electrodes (a) before and (b) after charge–discharge tests. Note the expansion in film thickness.

on charging (alloying), it does not return completely to its original geometry on discharging (de-alloying), and a large number of voids are created. As more and more Si particles lose contact with the CA on cycling, the impedance of the electrode rises.

Accordingly, increasing the CA content could have several positive effects in enhancing the cycling stability. First, it would reduce the chance of losing contact between the CA and Si particles. Second, a higher CA content will enable a better separation among Si particles, and thus decrease the possibility of particle agglomeration. The extraordinary volume expansion associated with large agglomerates of Si particles would be less reversible and hence more detrimental than small voids to the cycling stability. Finally, the soft nature of the CA materials may allow them to act as 'buffer', that, to some extent, can absorb the volume expansion and hence reduce the mechanical strain in the overall composite electrode.

The XRD pattern of the assembled Si electrode shows strong reflections of the underlying Cu substrate (Fig. 7). This indicates that the information collected is not solely from the surface but from throughout the entire Si-containing film. As Cu will not be consumed during cycling, its XRD reflections can serve as good internal standards for quantitative comparison of the XRD data of different electrodes. Through this approach, it is found that the XRD pattern remains almost unchanged after 30 cycles at a charging depth of 600 mAh per g-Si for the 3 μm–30% electrode. This result is in conflict with that previously reported by Yoshio et al. [1–3] from a study of carbon-coated Si particles. In that investigation, Si showed diminishing XRD intensities with cycling at a charging depth of 500 mAh g^{-1}, and could no longer be detected after 20 cycles. The intensity-diminishing effect was attributed to progressive amorphorization of Si particles upon repeated alloying–de-alloying processes. If the same amorphorization process had taken place in our electrode, the Si reflection intensities should have decreased with respect to either Cu or C reflections. The invariance of the Si XRD intensities therefore suggests that the de-alloying process of the un-coated Si particles results in crystalline Si. Whether or not the different results in this and the previous studies reside in the carbon layer coated on Si is being investigated.

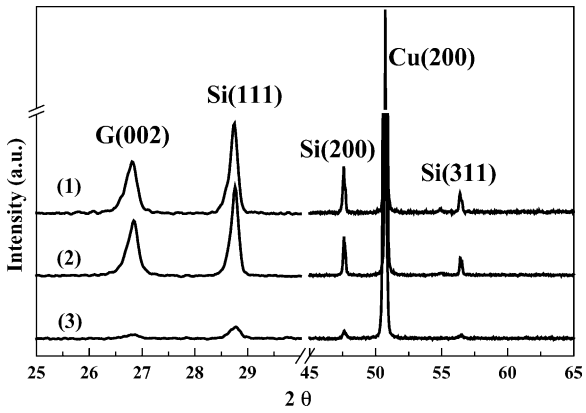

Fig. 7. X-ray diffraction patterns of Si electrode: (1) 3 μm–30%, fresh; (2) 3 μm–20%, after 30 cycles at charging depth of 600 mAh per g-Si and (3) 3 μm–15%, after 30 cycles. All patterns are normalized to same intensity for Cu(200). "G" stands for graphite.

By contrast, the decayed 3 μm–15% electrode shows a dramatic reduction in both Si and graphite XRD reflections. It is noted, however, that the Si and graphite peaks maintain approximately the same intensity ratio. Again, the intensity cannot be attributed to an amorphorization effect as this would cause intensity reduction for Si reflections but not for graphite ones. The intensity reduction observed in this decayed electrode is simply because the electrode became loose after cycling and part of it detached from the current-collector.

In summary, the effects of Si particle-size and CA content on the performance of the Si anode have been investigated. It is found that the CA content can have a profound effect on the cycle-life of the electrode, which increases with increasing CA content. Reducing Si particle-size, on the other hand, effectively facilitates the charging–discharging kinetics.

References

[1] M. Yoshio, H. Wang, K. Fukuda, T. Umeno, N. Dimov, Z. Ogumi, J. Electrochem. Soc. 149 (2002) A1598.
[2] N. Dimov, K. Fukuda, T. Umeno, S. Kugino, M. Yoshio, J. Power Sources 114 (2003) 88.
[3] N. Dimov, S. Kugino, M. Yoshio, Electrochim. Acta 48 (2003) 1579.
[4] J. Yang, B.F. Wang, K. Wang, Y. Liu, J.Y. Xie, Z.S. Wen, Electrochem. Solid State Lett. 6 (2003) A154.
[5] G.W. Zhou, H. Li, H.P. Sun, D.P. Yu, Y.Q. Wang, X.J. Huang, L.Q. Chen, Z. Zhang, Appl. Phys. Lett. 75 (1999) 2447.
[6] H. Li, X. Huang, L. Chen, G. Zhou, Z. Zhang, D. Yu, Y.J. Mo, N. Pei, Solid State Ionics 135 (2000) 181.
[7] P. Limthongkul, Y. Jang II, N.J. Dudney, Y.M. Chiang, Acta Mater. 51 (2003) 1103.
[8] M. Green, E. Fielder, B. Scrosati, M. Wachtler, J.S. Moreno, Electrochem. Solid State Lett. 6 (2003) A75.
[9] K. Seok II, G.E. Blomgren, P.N. Kumta, Electrochem. Solid State Lett. 6 (2003) A157.
[10] G.A. Robert, E.J. Cairns, J.A. Reimer, J. Power Sources 110 (2002) 424.
[11] G.X. Wang, L. Sun, D.H. Bradhurst, S. Zhong, S.X. Dou, H.K. Liu, J. Alloys Comp. 306 (2000) 249.
[12] K. Seok II, P.N. Kumta, G.E. Blomgren, Electrochem. Solid State Lett. 3 (2000) 493.